Synthesized-Reference-Wave Holography for Determining Antenna Radiation Characteristics

Vladimir Schejbal[1], Vlastimil Kovarik[2], and Dusan Cermak[1]

[1]University of Pardubice, Jan Perner Transport Faculty
Studentska 95, 53210 Pardubice, Czech Republic

[2]Retia, a.s.
Prazska 341, Zelene Predmesti, 530 02 Pardubice, Czech Republic
Tel: +420 466 036 293; Fax: +420 466 036 497;
E-mail: vladimir.schejbal@upce.cz, vkovarik@retia.cz, dusan.cermak@upce.cz

Abstract

Synthesized-reference-wave holographic techniques offer relatively simple and cost-effective measurement of antenna radiation characteristics and reconstruction of complex aperture fields using near-field intensity (power) pattern measurement. The near field is over-sampled. The phase is obtained indirectly, using the reference signal shifted linearly with the position of the probe. These methods allow utilization of advantages for probe compensation for near-field amplitude and phase measurements for planar and cylindrical scanning, including accuracy analyses. Descriptions are given of holographic near-field measurements using probe compensation for planar and cylindrical scanning, and numerical simulations. A comparison of holographic near-field and far-field measurements with and without probe compensation is presented.

Keywords: Antenna measurements; antenna radiation patterns; near-field sampling; near-field measurements; antenna probe compensation; holography

1. Introduction

Near-field measurements provide a fast and accurate method for determining the antenna's gain, pattern, polarization, beam pointing, etc. In contrast to conventional far-field methods, near-field antenna-measurement methods use a measuring probe in the radiating near-field region of the antenna under test (AUT). The far-field radiation pattern of the AUT must then be indirectly computed from the measurements made in the near-field region. Several methods for near-field antenna measurements have been proposed.

The standard complex (amplitude and phase) near-field measurements are used in the most common near-field technique. The methods use probe compensation for the amplitude and phase of the near-field measurements for planar and cylindrical scanning, and are well known [1-12]. However, the standard near-field measurement can be sensitive to phase-measurement errors. Moreover, the high cost of vector measurement equipment could limit accurate phase measurement at high frequencies. The problem of retrieving the full complex field distribution from the knowledge of amplitude data alone has therefore met with considerable interest, and many papers related to amplitude-only near-field measurements have been presented [13-28].

Indirect holographic imaging is a technique that has found widespread use at optical frequencies. It differs from standard complex (amplitude and phase) near-field measurements in that the complex fields are not measured directly, but are reconstructed from simple scalar measurements. This technique does have the advantage of not requiring the use an expensive vector analyzer, as only power measurement is required. It also enables the complex plane-wave spectrum and aperture fields of the AUT to be reconstructed from the measured scalar intensity pattern. The hologram is an interference pattern, produced by combining the signal from the AUT with a phase-coherent reference signal. The antenna's far-field patterns or aperture fields are then reconstructed from the recorded hologram. A disadvantage of this technique is that two terms containing information about the complex plane-wave spectrum are produced. These terms must be separated, in order to obtain the radiation characteristics of the AUT [17-19].

It is difficult to determine who first discovered the idea of synthesized-reference-wave holography (when the phase of the reference signal is shifted linearly with the position of the probe, and the near field is oversampled), which offers relatively simple and cost-effective solutions. This method overcomes the disadvantages of indirect holographic imaging. Certainly, reference [20] does not describe the new method. However, it gives new and interesting ideas and results for indirect holographic techniques. It also states

 ISSN 1045-9243/2008/$25 ©2008 IEEE

that similar ideas were suggested by Deschamps (1967). However, another publication can be considered [3], which cites Napier's PhD thesis (1971; see footnote 2), and [17, 21, and 22], which expand the ideas given for probe-compensated near-field measurements.

Synthesized-reference-wave holography was proposed in a PhD thesis [21] where several aspects were thoroughly analyzed (these methods allow utilizing the advantages of methods for probe compensation of amplitude and phase near-field measurements for planar and cylindrical scanning [1-12], including accuracy analyses). Most of the results have been published [22-28], such as a description of holographic near-field measurements using probe compensation for planar and cylindrical scanning, a comparison of holographic near-field and far-field measurements with and without probe compensation, accuracy analyses using mathematical models considering random processes with correlation intervals, numerical simulations considering random errors as well as deterministic errors, and processing of measurement statistics. On the other hand, references [22-28] contain not only results from PhD theses, but other results are added. This work summarizes some of the cited results (as some papers and the PhD theses are only in Czech), and gives some new results obtained by numerical simulations.

The validity of this technique was checked initially by numerical simulation, and later by experimental results. Cylindrical scanning was considered for radar fan-beam antenna testing [29, 30] and therefore very thorough analyses have been performed. Synthesized-reference-wave cylindrical surface measurements were carried out.

2. Near-Field Measurements for Planar and Cylindrical Scanning

Indirect holographic near-field measurements using a synthesized reference wave with probe compensation for planar and cylindrical scanning were derived [21, 22] considering well-known methods of probe compensation for amplitude and phase near-field measurements for planar and cylindrical scanning [1, 6]. A block diagram of synthesized-reference-wave holography is shown in Figure 1 [22], where the signal is recorded using a simple electric-field intensity (or possibly power) detector. It can be noted that this block diagram is basically the same as [20, Figure 4]. The reference wave is derived from the signal fed to the AUT by separating part of the signal fed to the AUT. This signal is fed forward via a transmission line, a phase shifter, and possibly a variable attenuator, to be combined with the sampled near-field signal of the AUT. The sampled near field is measured in exactly the same manner as used in conventional near-field measurements.
Considering one-dimensional scanning (along the x axis), and a synthesized reference signal with a linear phase change Ce^{-jax} (which simulates a plane wave propagating in the x direction with wavenumber a), the following equation for the output signal (formed by the sampled near field, $E(x)$, and the synthesized reference signal, Ce^{-jax}) can be obtained:

$$v(x)=\left|E(x)+Ce^{-jax}\right|^2 = \left|E(x)\right|^2+|C|^2+C^*E(x)e^{jax}+CE^*(x)e^{-jax}. \quad (1)$$

Depending on the equipment used, the received signal can be proportional to the power, $v(x)$, or to the electric field, $\sqrt{v(x)}$, when the resultant output power (or amplitude) is recorded. The amplitude of the reference signal, Ce^{-jax}, can be kept constant by a suitable adjustment of the reference-signal attenuation. It is approximately equal to the maximum of $E(x)$ ($|E(x)|<|C|$ is chosen). The required linear phase shift can be implemented by variation of the phase shifter. The term $|C|^2$ can be easily removed. Actually, it can be measured directly, if the AUT signal is disconnected or strongly attenuated. The Fourier transform of Equation (1), i.e., the complex plane-wave spectrum (PWS) with spatial frequency k_x, is

$$\mathbf{F}\left[v(x)\right] = \frac{1}{\sqrt{2\pi}}\int_{-\infty}^{\infty}\left[\left|E(x)\right|^2+|C|^2+C^*E(x)e^{jax}+CE^*(x)e^{-jax}\right]e^{-jk_x x}dx \quad (2)$$

This can be simplified for $|k_x|<k_1$ using a suitable constant a. Multiplying by e^{-jax} corresponds to a shift. If it is known that $\mathbf{F}\left[E(x)\right]=0$ for $|k_x|\ge k_2$ and $\mathbf{F}\left[\left|E(x)\right|^2\right]=0$ for $|k_x|\ge k_3$, then

$$\mathbf{F}\left[v(x)e^{-jax}\right]=\mathbf{F}\left[C^*E(x)\right] \quad (3)$$

for $|k_x|<k_1$, $2a>k_1+k_2$, $a>k_1+k_3$, as the other terms are equal to zero for $|k_x|<k_1$. The plane-wave spectrum can be shown to be bandlimited [1, 3]. Actually, the plane-wave spectrum becomes negligible beyond the limits $k_x^2=k^2=(2\pi/\lambda)^2$, where λ is the wavelength (for separation distances between the aperture and scanning planes of greater than a few wavelengths). Therefore, $k_1=k_2=k_3>k$ can be chosen. The described plane-wave spectrum and bandlimited properties are demonstrated by the numerical simulations given below.

The utilization of numerical methods of integration would be an approximation that introduces computational errors unless the sample increments approached zero. Fortunately, the relevant functions can be shown to be bandlimited, and thus sampling theo-

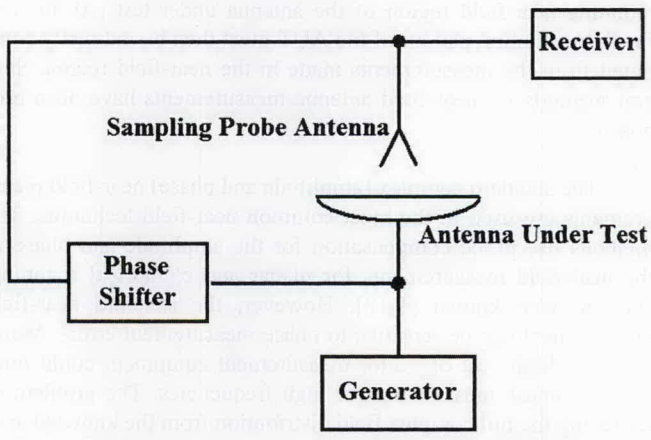

Figure 1. A block diagram of synthesized-reference-wave holography.

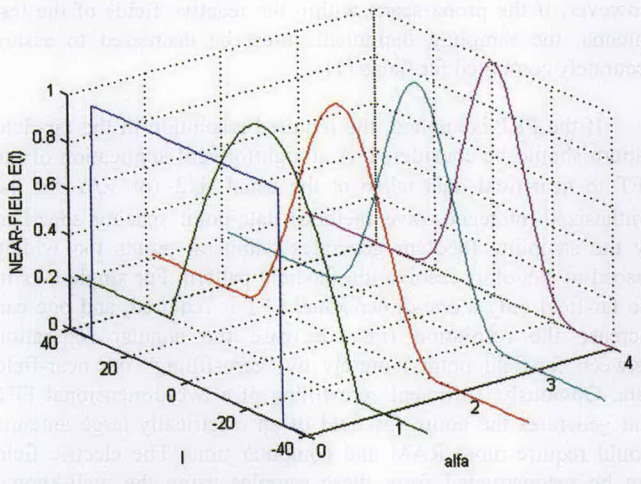

Figure 2. The input sequences (near-field distributions) $E(i)$.

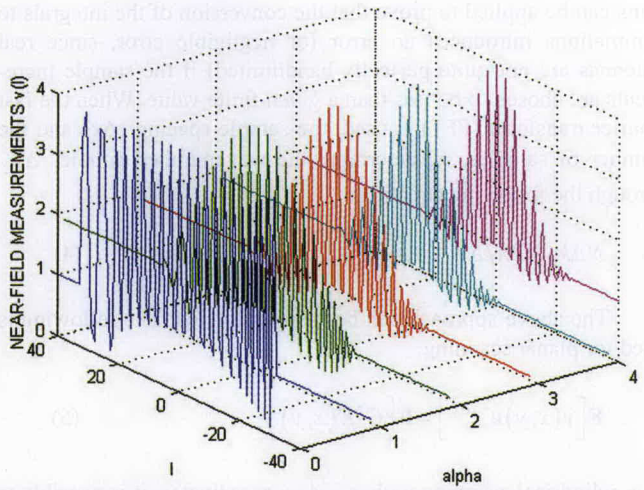

Figure 3. The near-field measurement simulations of $v(i)$.

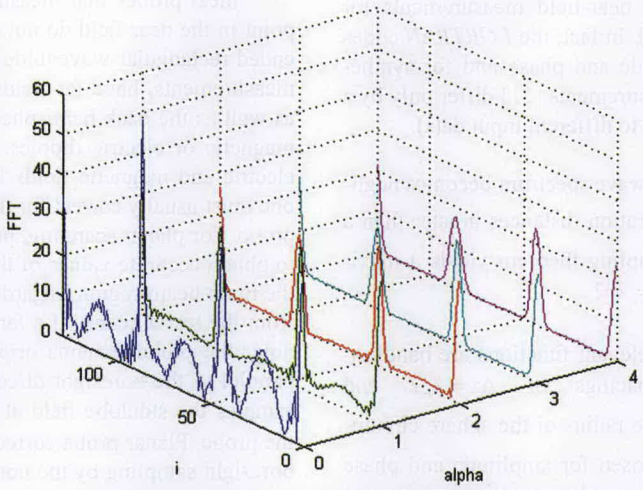

Figure 4. The FFT according to Equation (8).

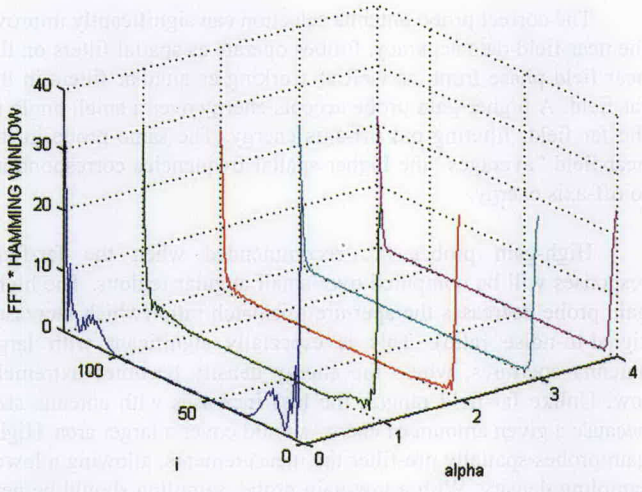

Figure 5. The plane-wave spectrum multiplied by the Hamming window spectra.

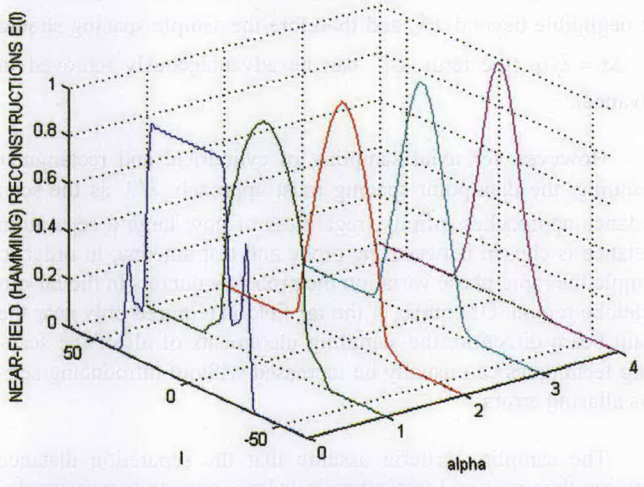

Figure 6. Near-field reconstructions using Hamming window spectra.

rems can be applied to prove that the conversion of the integrals to summations introduces no error (or negligible error, since real antennas are not quite perfectly bandlimited) if the sample increments are chosen to be less than a given finite value. When the fast Fourier transform (FFT) is used, the sample spacing, Δx, and the number of samples, N, determine the wavenumber sample, Δk_x through the following equation:

$$N\Delta k_x = 2\pi/\Delta x. \tag{4}$$

The above approach can be easily extended. The following is used for planar scanning:

$$\mathbf{F}\left[v(x,y)e^{-jax}\right] = \mathbf{F}\left[C^*E(x,y)\right]. \tag{5}$$

For cylindrical scanning with r_0, ϕ, z coordinates, it is possible to write

$$\mathbf{F}\left[v(r_0,\phi,z)e^{-jaz}\right] = \mathbf{F}\left[C^*E(r_0,\phi,z)\right]. \tag{6}$$

This allows using the advantages of the methods for probe compensation for amplitude and phase near-field measurements for planar and cylindrical scanning [1, 6]. In fact, the *FORTRAN* codes for cylindrical scanning for amplitude and phase and for synthesized-reference-wave near-field measurements [21] differ only by a few lines (most changes are due only to different input data).

For planar scanning, the plane-wave spectrum becomes negligible beyond $k_x^2 + k_y^2 = k^2$ (for separation distances greater than a few wavelengths), and thus the sampling theorem yields a maximum data-point spacing of $\Delta x = \Delta y = \lambda/2$.

For cylindrical scanning, the relevant functions are bandlimited as well, and sample spacings of $\Delta z = \lambda/2$ and $\Delta\phi = \left[\lambda/2(r_m + \lambda)\right]$, where r_m is the radius of the sphere circumscribing the test antenna, can be chosen for amplitude and phase measurements. This means that the angular sampling increments for cylindrical scanning are independent of the scan radius, r_0.

Similarly, the sampling criteria can be applied to fulfill the assumptions of Equation (2). In this case, oversampling should be used, as the plane-wave spectrum of any (non-shifted) term should be negligible beyond k^2, and therefore the sample spacing should be $\Delta x = \lambda/6$ (the term $|C|^2$ can be advantageously removed in advance).

However, for axial sampling of cylindrical and rectangular scanning, the data-point spacing must approach $\lambda/2$ as the scan distance approaches infinity, regardless of how large a separation distance is chosen between the probe and test antenna, in order to sample the rapid phase variation the probe encounters in the far-out sidelobe region. Of course, if the far field is required only near the main beam direction, the sampling increments of all of the scanning techniques can usually be increased without introducing serious aliasing errors.

The sampling criteria assume that the separation distance between the probe and test antennas is large enough to prevent significant coupling of their reactive fields. For non-super-reactive antennas, a few wavelengths of separation are usually sufficient. However, if the probe scans within the reactive fields of the test antenna, the sampling increments must be decreased to assure accurately computed far fields [1].

If the FFT is applied, the required resolution in the far-field pattern should be considered. A straightforward application of the FFT to near-field data taken at the usual $\lambda/2$ (or $\lambda/6$ for the synthesized-reference-wave method) data-point spacing specified by the sampling theorem generates output at points too widely spaced to smoothly resolve the far-field pattern. For single cuts in the far-field only a one-dimensional FFT is required, and one can increase the resolution (i.e., decrease the angular separation between far-field points) merely by "zero-filling" the near-field data. Obviously, sufficient zero-filling of a two-dimensional FFT that generates the entire far field of an electrically large antenna would require more RAM and computer time. The electric field can be reconstructed from these samples using the well-known sampling theorem [1], as well. Generally, the post-processing can be done at any time after measurement, and/or another computer could be used for the post-processing. It is not necessary to explain that the progress of hardware and software allows the utilization of modern "user-friendly" tools.

Ideal probes that measure the electric or magnetic field at a point in the near field do not exist, in practice. For example, open-ended rectangular-waveguide probes, commonly used in near-field measurements, have far fields that differ appreciably (in the front as well as the back hemispheres) from the far fields of elementary magnetic or electric dipoles. Thus, for accurate determination of electric and magnetic fields from measurements in the near field, one must usually correct for the non-ideal receiving response of the probe. For planar scanning, probe correction is generally necessary to obtain accurate values of the far field of the test antenna outside the main-beam region, regardless of how far the probe is separated from the test antenna (if a far field is not used). With planar scanning, the probe remains oriented in the same direction (usually, parallel to the boresight direction of the test antenna), and thus it samples the sidelobe field at angles off the boresight direction of the probe. Planar probe correction simply compensates for this off-boresight sampling by the non-ideal probe of the plane waves radiated by the test antenna. For cylindrical scanning, the same argument can be applied in the axial scanning direction to explain why probe correction is generally necessary for cylindrical near-field measurements, regardless of the separation distance between the test and probe antennas [3].

The correct probe-antenna selection can significantly improve the near-field data accuracy. Probes operate as spatial filters on the near-field phase front, as well as working as angular filters in the far field. A higher-gain probe accepts energy over a small angle in the far field, filtering out off-axis energy. The same probe in the near-field "averages" the higher spatial frequencies corresponding to off-axis energy.

High-gain probes are recommended when the far-field responses will be computed over small angular regions. The high-gain probe decreases the aperture-mismatch ratio (which increases signal-to-noise ratio). This is especially significant with large antenna apertures, where the energy density becomes extremely low. Unlike far-field ranges, the loss increases with antenna size because a given amount of energy should cover a larger area. High-gain probes spatially pre-filter the measurements, allowing a lower sampling density. With a low-gain probe, sampling should be performed at less than $\lambda/2$ spacing to satisfy the sampling criteria. With high-gain probes, a sampling density of 0.2 samples per

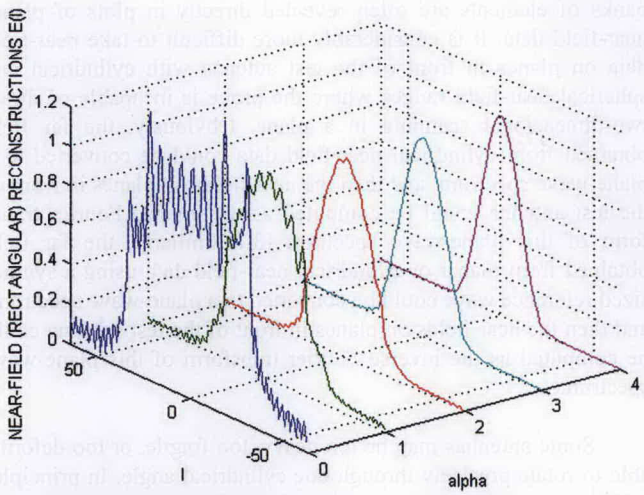

Figure 7. Near-field reconstructions using a rectangular window.

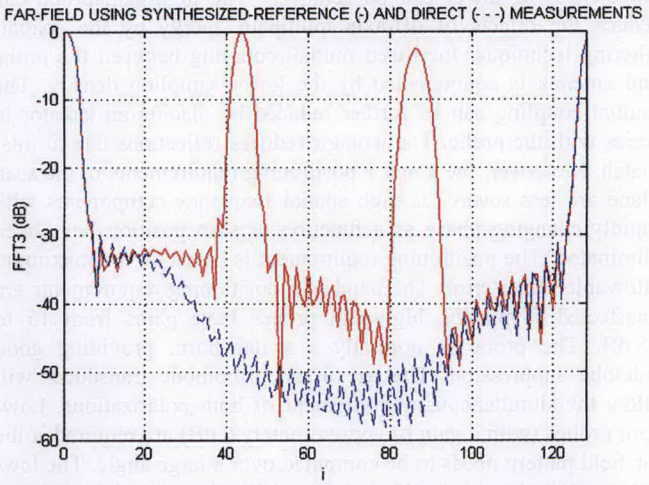

Figure 8. Far-field amplitudes obtained by synthesized-reference-wave holography (solid line) and direct near-field measurements for $\alpha = 3$.

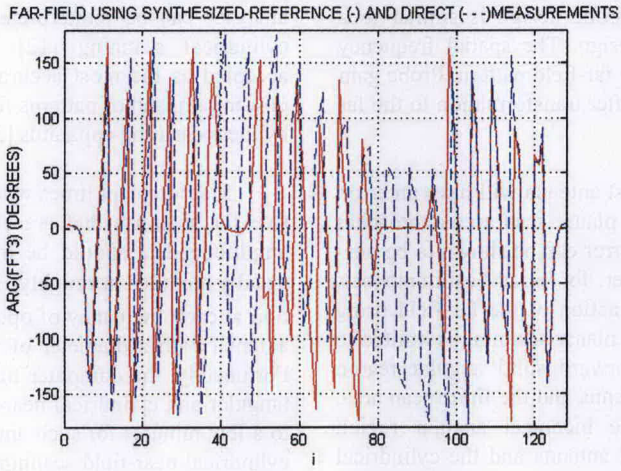

Figure 9. Far-field phases obtained by synthesized-reference-wave holography (solid line) and direct near-field measurements for $\alpha = 3$.

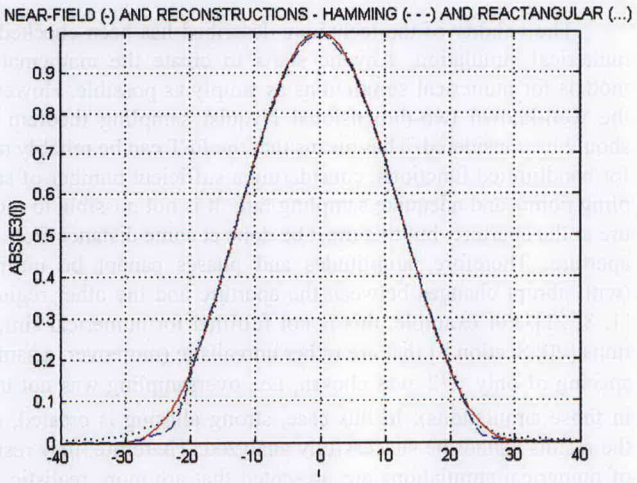

Figure 10. Near-field amplitudes (solid line) and reconstructions using Hamming (- - -) and rectangular (•••) windows for $\alpha = 3$.

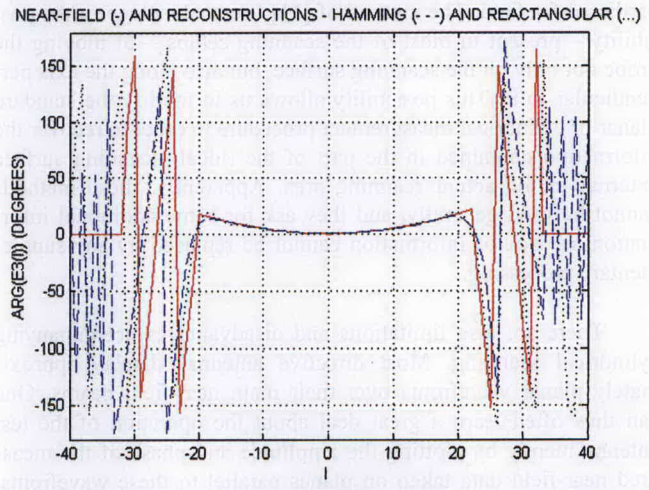

Figure 11. Near-field phases (solid line) and reconstructions using Hamming (- - -) and rectangular (•••) windows for $\alpha = 3$.

wavelength or lower can be achieved. The high-gain probe can reduce the effects of off-axis multipath energy by the spatial-filtering technique. Increased mutual coupling between the probe and antenna is counteracted by the lower sampling density. The mutual coupling can be further reduced by placing an isolator in series with the probe. The isolator reduces reflections due to mismatch. Moreover, the x and y positioning requirements in the scan plane are less severe, as high spatial frequency components with rapidly changing phase as a function of scan position have been eliminated. The positioning requirement is based on the maximum allowable phase error. The axial or z positioning requirements are unaffected. Typically, high-gain probes have gains from 15 to 25 dB. The probe is normally a scalar horn, providing good sidelobe suppression. The use of an orthomode transducer will allow the simultaneous measurement of both polarizations. Low-gain probes (with a gain of approximately 6 dB) are required if the far-field pattern needs to be computed over a large angle. The low-gain probes do not significantly spatially filter the data. Typical probes are open-ended waveguide sections. For high-quality measurements of deep sidelobes, a probe with an axial null is preferred. This type of probe operates as either a high-pass or a band spatial frequency rejecting the main beam. The result is a reduced receiver linearity requirement, since the overpowering main-beam contribution is not present. The physical probe design is similar to a monopulse (auto track) feed horn design. The spatial frequency filtering of the RF probes modifies the far-field pattern. Probe gain correction can be applied prior to or after transformation to the far field to eliminate gain errors [4].

The computed far field of the test antenna will have an error, which does not approach zero as the planar scan area approaches infinity. In practice, this planar-scan error can be shown to be negligible for directive antennas. However, for broad-beam antennas, this can prevent the accurate determination of the far field using planar near-field scanning. In general, planar scanning is limited to determining the fields within the forward solid angular region subtended by the edges of the test antenna and the finite scan area. Cylindrical scanning omits only the biconical angular region formed by the outer edges of the test antenna and the cylindrical scan area of finite height. The method of [10] uses a priori information on the geometry of the AUT and on the overall precision of the acquired data to estimate the near field outside the available scan area. The far-field pattern is then evaluated from the estimated near-field data using a standard near-field/far-field algorithm, resulting in a considerable extension of the angular range for the predicted far field. The method of [11] takes advantage of the possibility – present in most of the scanning setups – of moving the probe not only on the scanning surface, but also along the axis perpendicular to it. This possibility allows us to modify the standard planar or cylindrical measurement procedure in order to recover the information contained in the part of the (ideal) scanning surface external to the actual scanning area. Apparently, these methods cannot be used generally, and they ask for some additional information, as lack of information cannot be replaced by any supplementary processing.

There are also limitations and disadvantages accompanying cylindrical scanning. Most directive antennas display approximately planar wavefronts over their main near-field beams. One can thus often learn a great deal about the operation of the test antenna merely by plotting the amplitude and phase of the measured near-field data taken on planes parallel to these wavefronts. For instance, it is possible to align the panels of a millimeter-wave reflector by plotting the phase contours of near-field data taken on a plane in front of the reflector. Similarly, faulty array elements or banks of elements are often revealed directly in plots of planar near-field data. It is considerably more difficult to take near-field data on planes in front of the test antenna with cylindrical and spherical near-field ranges where the probe is incapable of direct two-dimensional scanning in a plane. Obviously, the far field obtained from cylindrical near-field data could be converted to a plane-wave spectrum, and then the near fields on planes in front of the test antenna could be computed as the inverse Fourier transform of this plane-wave spectrum [3]. Similarly, the far field obtained from planar or cylindrical near-field data using a synthesized reference wave could be converted to a plane-wave spectrum, and then the near fields on planes in front of the test antenna could be computed as the inverse Fourier transform of this plane-wave spectrum.

Some antennas may be too heavy, too fragile, or too deformable to rotate precisely through one cylindrical angle. In principle, cylindrical scanning could still be applied for such antennas by fixing the antenna and moving the probe on a cylinder surrounding the antenna. Although much progress has been made in simplifying the probe correction for cylindrical near-field scanning, this remains more difficult to formulate, understand, and apply than for planar scanning. In addition, the results from the planar error analyses can be reinterpreted to estimate the effect of errors in cylindrical scanning [12]. The near-field technique may be accepted as the most accurate technique for the measurement of power gain, and of patterns for antennas that can be accommodated by the measuring apparatus [3].

Measurement times would make near-field scanning unattractive for antennas that are electrically extremely large. Since the amplitude data should be oversampled, and therefore should be usually recorded at roughly $\lambda/6$ in the near field for each polarization at each frequency of operation, it would take hours to scan an antenna with a diameter of more than one hundred wavelengths. Fortunately, the computer time required for processing plane rectangular and cylindrical near-field scanning data typically amounts to a few minutes for such antennas, and thus plane-rectangular and cylindrical near-field scanning could be measurement-time limited rather than computer-time limited.

3. Numerical Simulations

The validity of the technique described has been checked by numerical simulation. Anyone starts to create the mathematical models for numerical simulations as simply as possible. However, the well-known two-dimensional Nyquist sampling theorem [1] should be considered. That means that the FFT can be reliably used for bandlimited functions, considering a sufficient number of sampling points and adequate sampling rate. It is not possible to measure at the aperture, but this must be done at some distance from the aperture. Therefore, amplitudes and phases cannot be uniform (with abrupt changes between the aperture and the other regions) [1, 8, 21]. For example, this is not fulfilled for numerical simulations [20, Section 5] that are rather unrealistic (moreover, a sample spacing of only $\lambda/2$ was chosen, i.e., oversampling was not used in those simulations). In this case, strong aliasing is created, and the results cannot be successfully analyzed. Therefore, new results of numerical simulations are presented that are more realistic. As one case of the proposed simulations is not realistic, it is possible to compare various input sequences (near-field distributions) to demonstrate that effect.

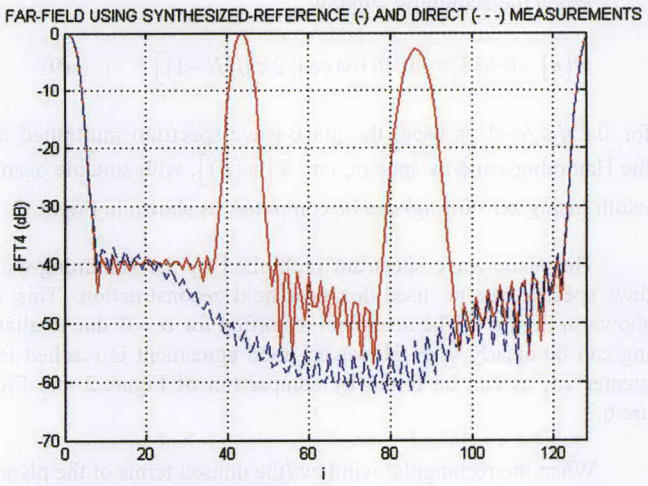

Figure 12. Far-field amplitudes obtained by synthesized-reference-wave holography (solid line) and direct near-field measurements for $\alpha = 4$.

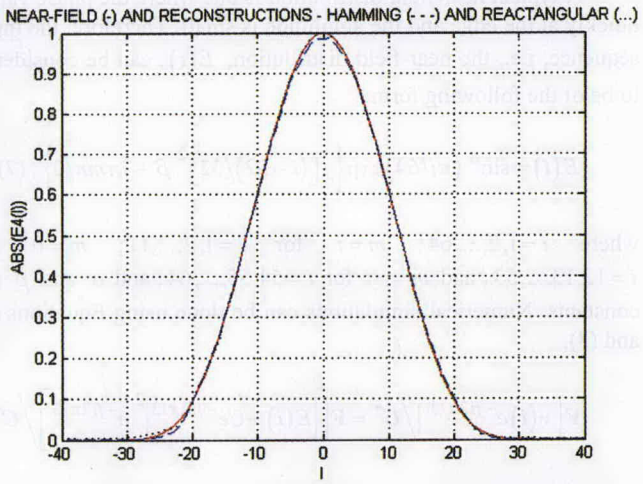

Figure 14. Near-field amplitudes (solid line) and reconstructions using Hamming (- - -) and rectangular (•••) windows for $\alpha = 4$.

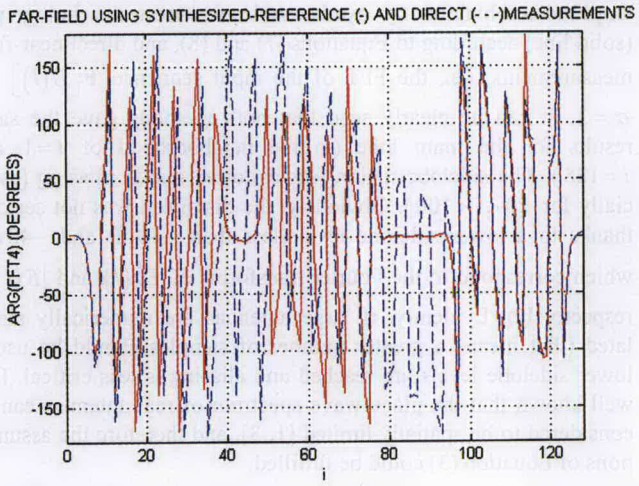

Figure 13. Far-field phases obtained by synthesized-reference-wave holography (solid line) and direct near-field measurements for $\alpha = 4$.

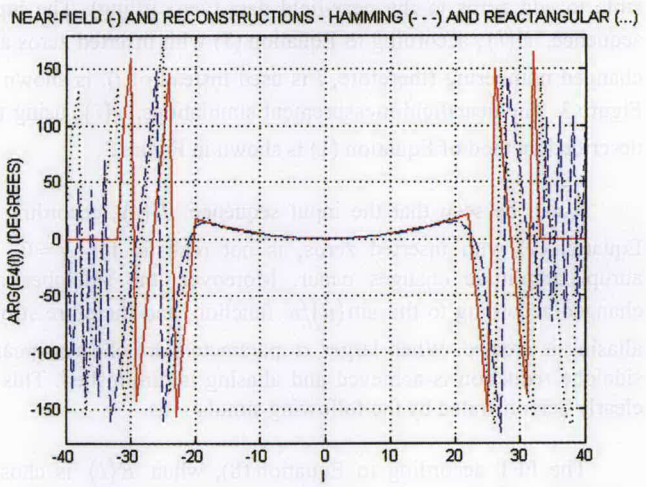

Figure 15. Near-field phases (solid line) and reconstructions using Hamming (- - -) and rectangular (•••) windows for $\alpha = 4$.

A typical near-field distribution is one where the phase varies quickly at the edge and the amplitude is small. Therefore, the input sequence, i.e., the near-field distribution, $E(i)$, can be considered to be of the following form:

$$E(i)=\sin^{\alpha}(\pi i/64)\exp\left\{j\left[(i-32)/32\right]^2\beta+j\pi mn/3\right\}, \quad (7)$$

where $i=1,2,...,64$; $m=i$ for $i=1,2,...,11$; $m=0$ for $i=12,13,...,53$; and $m=-i$ for $i=54,55,...,64$; and α and β are constants. Numerical simulations can be done using Equations (1) and (3),

$$\mathbf{F}\left[v(i)e^{-ji2\pi/3}\right]/C^{*}=\mathbf{F}\left[\left|E(i)+Ce^{-ji2\pi/3}\right|^2 e^{-ji2\pi/3}\right]/C^{*}$$

$$=\mathbf{F}\left[E(i)\right], \quad (8)$$

for a region of space where the electromagnetic field contains no evanescent waves (the far field of an antenna). Considering this region, the near-field distribution, $E(i)$, could be obtained by the inverse Fourier transform. Some of the numerical simulation results are shown for $\beta=\pi/4$. To increase the resolution (i.e., decrease the angular separation between far-field points), it is possible to add zeros to the near-field data (zero filling). The input sequence, $E(l)$, according to Equation (7) with inserted zeros and changed numbering (therefore, l is used instead of i), is shown in Figure 2. The near-field measurement simulations, $v(i)$, using the described method of Equation (1) is shown in Figure 3.

It can be seen that the input sequence, $E(l)$, according to Equation (7) with inserted zeros, is not realistic for $\alpha=0$, as abrupt amplitude changes occur. Moreover, the sidelobes are changed according to the $\sin(u)/u$ function, and therefore strong aliasing is created. When larger α parameters are chosen, greater sidelobe reduction is achieved and aliasing is diminished. This is clearly demonstrated by the following simulations.

The FFT according to Equation (8), when $E(l)$ is chosen according to Equation (7) and $|C|^2$ is removed, is shown in Figure 4. The three terms of Equation (2) can be clearly distinguished (with maxima for $i=1$, $i\approx 42$, and $i\approx 85$). The most important part of the plane-wave spectrum (from the far-field radiation pattern point of view) is in the neighborhood of $i=1$ (and, thanks to the periodic properties of the FFT, $i=128$), when $\mathbf{F}\left[E(l)\right]$ is obtained. Obviously, the assumptions of Equation (3) cannot be theoretically satisfied and aliasing can occur. The assumptions of Equation (3) can be practically fulfilled when greater sidelobe reductions are reached.

Various windows can be used to filter the remainder terms. It is not possible to determine the best window in advance. It could appear that the best choice is the rectangular window when the unused terms of the plane-wave spectrum are equal to zero. That can be used when only the far field is considered, as the inverse Fourier transform (for near-field reconstruction) would create a $\sin(u)/u$ pattern (see below). The properties of the plane-wave spectrum filter were considered in [1], where the Blackman filter was analyzed.

When the Hamming window,

$$w(n)=0.53836-0.46164\cos\left[2\pi n/(N-1)\right] \quad (9)$$

for $0\le n\le N-1$ is used, the plane-wave spectrum multiplied by the Hamming-window spectra, i.e., $\mathbf{F}\left[w(n)\right]$, with suitable beamwidth (using zero filling) can be computed, as shown in Figure 5.

The plane-wave spectrum multiplied by the Hamming-window spectra can be used for near-field reconstruction. This is shown in Figure 6. The near-field distortion for $\alpha=0$ due to aliasing can be clearly seen. However, good agreement is reached for greater α, as can be found by comparison of Figure 2 and Figure 6.

When the rectangular window (the unused terms of the plane-wave spectrum are equal to zero) is used for near-field reconstruction, $\sin(u)/u$ patterns for the inverse Fourier transform are created, and greater near-field distortions due to aliasing can be clearly seen. This is true not only for $\alpha=0$, but even for $\alpha=1$, as can be found by comparison of Figure 2 and Figure 7, where near-field reconstructions using rectangular window are shown.

Detailed comparisons can be done for any α. As an example, this was done for α equal to 3 and 4. Figure 8 shows far-field amplitudes obtained by synthesized-reference-wave holography (solid line) according to Equations (7) and (8), and direct near-field measurements, i.e., the FFT of the input sequence $\mathbf{F}\left[E(l)\right]$ for $\alpha=3$. It can be clearly seen that both methods gave the same results for the main lobe (in the neighborhood of $i=1$ and $i=128$). The sidelobe region was distorted due to aliasing (especially for $20<i<100$). Obviously, the distortion was not serious, thanks to a lower sidelobe level (less than -30 dB and -40 dB, which correspond to the Fourier transforms of $E^{*}(l)$ and $|E(l)|^2$, respectively). Evidently, if large antennas are numerically simulated (that means a greater number of samples should be used), lower sidelobe levels are reached and aliasing is less critical. It is well known that the plane-wave spectrum of real antennas can be considered to be spatially limited [1, 3], and therefore the assumptions of Equation (3) could be fulfilled.

Similarly, Figure 9 shows far-field phases obtained by synthesized-reference-wave holography (solid line) according to Equations (7) and (8), and direct near-field measurements, i.e., the FFT of the input sequence $\mathbf{F}\left[E(l)\right]$ for $\alpha=3$. It can be clearly seen that both methods gave the same results for the main lobe (in the neighborhood of $i=1$ and $i=128$). The sidelobe region was distorted due to aliasing (especially for $20<i<100$). Obviously, the distortion was not serious, thanks to a lower sidelobe level. If large antennas were numerically simulated, then lower sidelobe levels would be reached and aliasing would be less critical.

Near-field amplitudes are shown by the solid line in Figure 10 for $\alpha=3$. Obviously, when the FFT and then the inverse FFT of the input sequence $E(l)$ is performed, the result should be the same. The amplitude reconstructions using the Hamming (- - -) and rectangular (• • •) windows are shown for comparison. The near-field amplitudes and amplitude reconstructions were nearly the same. Similarly, near-field phases are shown by the solid line in Figure 11 for $\alpha=3$. The phase reconstructions using the Hamming (- - -) and rectangular (• • •) windows are shown for comparison.

The near-field phases and phase reconstructions were very similar, but perfect agreement was not reached. However, it could be considered that these discrepancies were due to aliasing, as the spectra were not exactly the same (compare the amplitudes and phases of the individual spectra in Figures 8 and 9). On the other hand, it is difficult to determine which reconstruction was better (or possibly to select the most suitable window).

Figure 12 shows far-field amplitudes obtained by synthesized-reference-wave holography (solid line) according to Equations (7) and (8) and direct near-field measurements, i.e., the FFT of the input sequence $\mathbf{F}\left[E(l)\right]$ for $\alpha = 4$. It can be clearly seen that both methods gave the same results for the main lobe (in the neighborhood of $i = 1$ and $i = 128$). The sidelobe region was distorted due to aliasing (especially for $20 < i < 100$). Obviously, the distortion was not serious thanks to a lower sidelobe level (about -40 dB). Similarly, Figure 13 shows the far-field phases obtained by synthesized-reference-wave holography (solid line) according to Equations (7) and (8) and direct near-field measurements, i.e., the FFT of the input sequence $\mathbf{F}\left[E(l)\right]$ for $\alpha = 4$. It can be clearly seen that both methods gave the same results for the main lobe (in the neighborhood of $i = 1$ and $i = 128$). The sidelobe region was distorted due to aliasing (especially for $20 < i < 100$). Obviously, the distortion was not serious thanks to the lower sidelobe level. Thanks to the lower sidelobe levels (compared with the case for $\alpha = 3$), the aliasing was less critical.

Near-field amplitudes are shown by the solid line in Figure 14 for $\alpha = 4$. The amplitude reconstructions using the Hamming (- - -) and rectangular (• • •) windows are shown for comparison. Similarly, the near-field phases are shown by the solid line in Figure 15 for $\alpha = 4$. The phase reconstructions using the Hamming (- - -) and rectangular (• • •) windows are shown for comparison. As for the previous example (with lower α), the near-field phases and phase reconstructions were very similar, but perfect agreement was not reached. However, it could be considered that these discrepancies were due to aliasing, as the spectra were not exactly the same (compare the amplitudes and phases of the individual spectra in Figures 12 and 13). Thanks to the lower sidelobe levels (compared to the case for $\alpha = 3$), the aliasing was less critical. On the other hand, it was also difficult to determine which reconstruction was better (or, possibly, to select the most suitable window).

Obviously, if large antennas are numerically simulated (that means a greater number of samples should be used), lower sidelobe levels are reached and aliasing is less critical. It is well known that the plane-wave spectrum of real antennas can be considered to be spatially limited [1], and therefore the assumptions of Equation (3) could be fulfilled. Therefore, better agreement between near-field and relevant reconstructions could be expected. Generally, the far-field-to-near-field transformations are not correct, as (generally unknown) radiation sources are present inside the far-field region. However, the AUT structure is known a priori, and therefore reconstructions using suitable surfaces and windows could be justified, as it is demonstrated by the given numerical simulations.

4. A Comparison of Holographic Near-Field and Far-Field Measurements

Very useful near-field measurement comparisons of conventional (amplitude and phase) and synthesized-reference-wave methods can be found in [20]. Even though comparisons with radiation patterns measured on conventional far-field ranges would not give a reliable evaluation of near-field techniques [8], it could be very useful when far-field measurements of medium antennas are performed in an anechoic chamber. Therefore, comparisons of holographic near-field measurements using synthesized-reference-wave and far-field measurements on a cylindrical surface, with and without probe compensation, have been done [21, 25] (where the detailed equipment description can be found). Only some of these measurements are shown. The AUT was measured by two different probes, an electric dipole and an open-ended waveguide, for basic and cross polarization, and for various sample distances. The measurement equipment was relatively simple, and various errors were created, such as probe-alignment and position errors. On the other hand, this allowed accuracy analyses using statistical processing of data obtained experimentally, and comparison with accuracy analyses using mathematical models considering random processes with correlation intervals [21].

If the sample spacing is $\Delta z \le \lambda/6$ and $a\Delta z = 2\pi/3$, then the space period is $N\Delta k_z = 2\pi/\Delta z \ge 12\pi/\lambda$ and $\alpha \ge 4\pi/\lambda$, and the assumptions of Equation (3) are clearly fulfilled. With a phase increment of $2\pi/3$, the phase state was repeated every third line. In practice, this meant that the phase-shifter settings only needed to be changed on three occasions throughout the overall scan (data could be taken for line 1, line 4, line 7, etc., for a zero shifter setting, for line 2, line 5, line 8, etc., for a $2\pi/3$ shifter setting, and for line 3, line 6, line 9, etc., for a $4\pi/3$ shifter setting) [20].

A five-element waveguide-slot array was measured for $\lambda = 32$ mm. Near-field measurements with cylindrical scanning, a

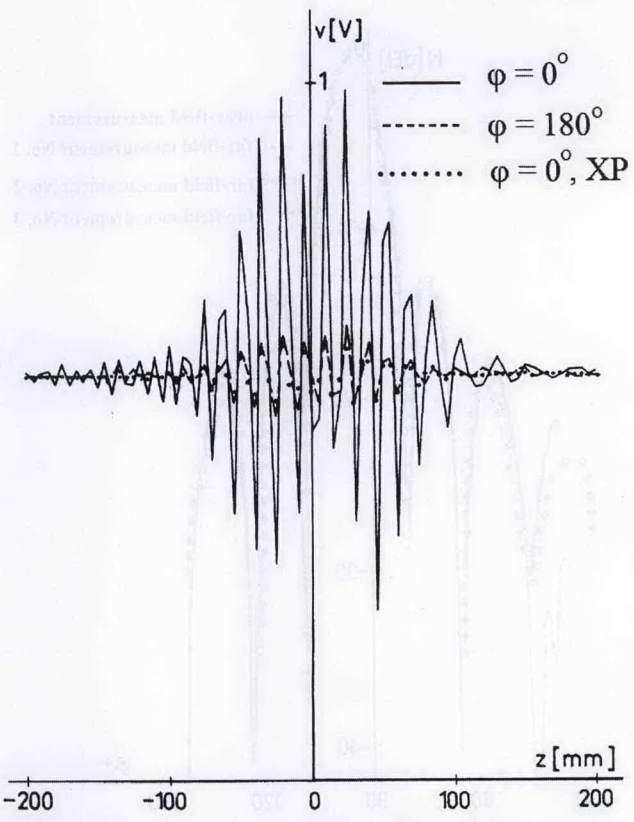

Figure 16. Near-field measurements with cylindrical scanning, a dipole probe, and $\Delta = 5$ mm.

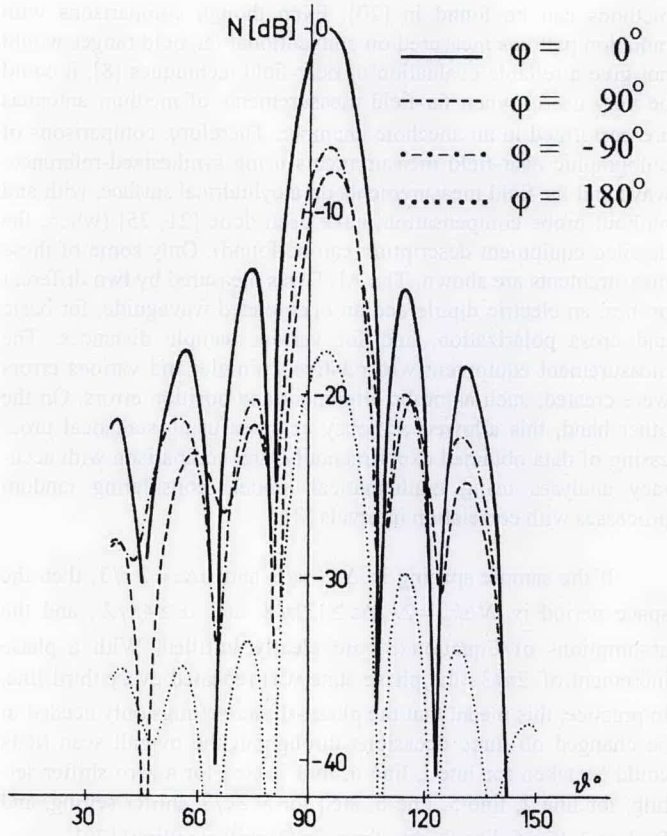

Figure 17. Calculated far-field radiation patterns for near-field measurements with $\Delta = 5$ mm and $-200 \le z \le 200$ mm.

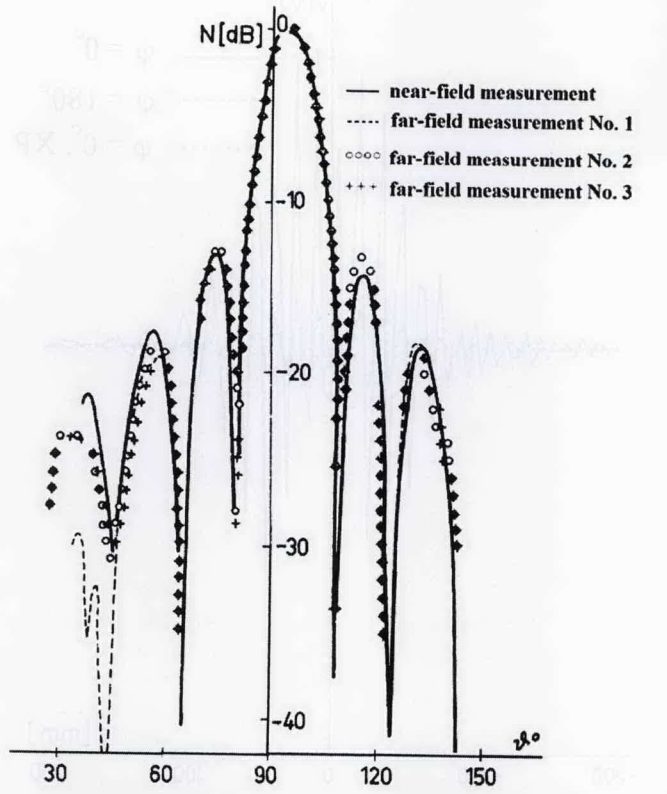

Figure 18. A comparison of near-field and far-field measurements for $\phi = 0°$.

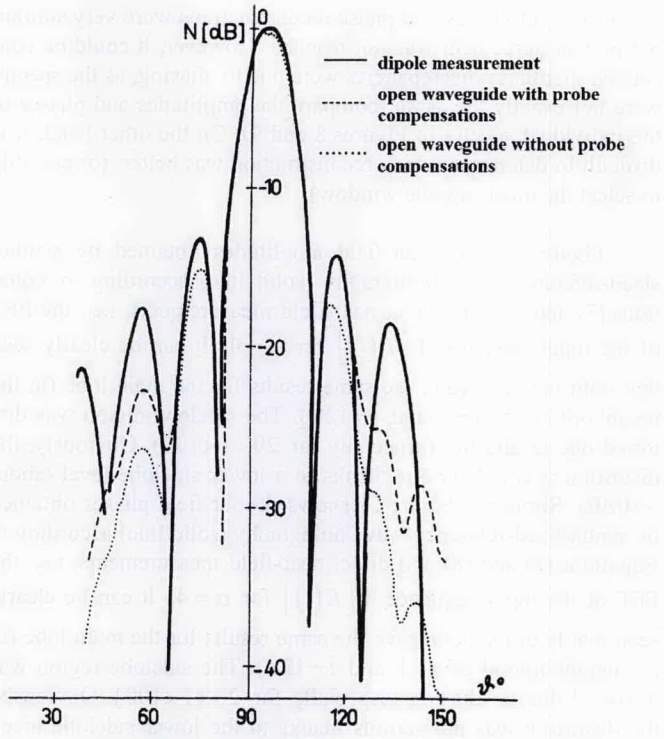

Figure 19. A comparison of near-field measurements for $\phi = 0°$ (the open-waveguide probe calculation was not reliable for $\vartheta < 65°$ and $\vartheta > 115°$).

dipole probe, and $\Delta z = 5$ mm for various planes $\phi = \text{const.}$ are shown in Figure 16 (XP is a cross polarization).

Calculated far-field radiation patterns using Equation (6) and the probe-compensation method [6] for the open-ended waveguide are shown in Figure 17 for near-field measurements with $\Delta z = 5$ mm and $-200 \text{ mm} \le z \le 200$ mm. For the far-field calculation, 128 points were considered (zero received signal, i.e., the reference wave Ce^{-jax}, was only used for $|z| > 200$ mm).

A comparison of near-field and far-field measurements for $\phi = 0°$ is shown in Figure 18. The small differences between individual far-field measurements were created by various measurement conditions. Far-field measurement 1 was performed with a different arrangement of feeding waveguides. Measurements 2 and 3 were performed with the same arrangement of feeding waveguides as for the near-field measurements. However, measurement 2 was performed without absorbers on the floor, and therefore the sidelobe levels were slightly higher. The reasonable agreement among the various near-field and far-field measurements can be noted.

A comparison of radiation patterns for $\phi = 0°$ calculated from near-field measurements with a dipole probe (without probe compensation) and an open-waveguide probe with and without probe compensation are shown in Figure 19. Excellent agreement between the radiation patterns determined from the dipole measurement and the open-waveguide with probe compensation in the vicinity of $\vartheta = 90°$ was achieved. The calculation without the open-waveguide probe compensation differs from the other calculations (especially for the sidelobe regions). It is well known [8] that the planar scan technique does not give information about the field outside the solid angle γ_{max}, formed by the edge of the aper-

ture antenna and the boundary of the scan antenna, i.e., the calculation is not reliable for $\vartheta < 90° - \gamma_{max}$ and $\vartheta > 90° + \gamma_{max}$. The γ_{max} angles were different, due to various r_0 distances between the z axis and the probe and the z coordinate intervals. The values were 63° for the dipole probe and 25° for the open-waveguide probe, i.e., the calculation was not reliable for $\vartheta < 65°$ and $\vartheta > 115°$ for the open-waveguide probe.

5. Conclusions

Near-field antenna measurement methods, in contrast to conventional far-field methods, use a measuring probe in the radiating near-field region of the AUT. The interest in near-field measurements has been generated primarily by the development of modern, specially designed antennas that are not easily measured on conventional far-field ranges. Plenty of examples where near-field antenna measurements could be more advantageous have been published.

Methods that use probe compensation for amplitude and phase near-field measurements for planar, cylindrical, and spherical scanning are well known. The high cost of vector measurement equipment could limit accurate phase measurement at high frequencies. Moreover, the standard near-field measurement can be sensitive to phase-measurement errors. Therefore, the problem of obtaining the full complex field distribution from a knowledge of the amplitude data alone has met with considerable interest.

Holographic imaging is a technique that has found widespread use at optical frequencies. It differs from amplitude and phase near-field measurements, as the complex fields are not measured directly but are reconstructed from simple scalar measurements. This technique does not require the use of an expensive vector analyzer, as only a field power (amplitude) measurement is required, and the antenna's far-field patterns or aperture fields can be reconstructed from the recorded hologram. The idea of synthesized-reference-wave holography, which offers relatively simple and cost-effective solutions, overcomes some of the holographic imaging disadvantages. Synthesized-reference-wave holography, which expands the ideas for probe-compensated near-field measurements, has been proposed, and several aspects have been thoroughly analyzed. These methods allow employing the advantages of methods for probe compensation for amplitude and phase near-field measurements for planar and cylindrical scanning, including accuracy analyses. Synthesized-reference-wave holographic techniques offer measurements of antenna radiation characteristics and reconstruction of complex aperture fields using near-field intensity-pattern measurements. The validity of this technique has been checked by numerical simulation as well as experimental results. Even though the *FORTRAN* code for planar scanning has been debugged, it has not been extensively tested, as it is not very suitable for radar fan-beam antennas. Cylindrical scanning is advantageous for radar fan-beam antenna testing, and therefore it has been considered and very thoroughly analyzed. Synthesized-reference-wave cylindrical surface measurements were carried out, and a comparison of holographic near-field and far-field measurements with and without probe compensation was presented.

6. Acknowledgements

The paper was supported by the Czech National Institutional Research "Theory of Transport System" No. MSM 0021627505.

7. References

1. E. B. Joy and D. T. Paris, "Spatial Sampling and Filtering in Near-Field Measurements," *IEEE Transactions on Antennas and Propagation*, **AP-20**, 3, May 1972, pp. 253-261.

2. A. D. Yaghjian, "Near-Field Antenna Measurements on a Cylindrical Surface: A Source Scattering-Matrix Formulation," National Bureau of Standards Technical Note 696. Boulder, September 1977.

3. A. D. Yaghjian, "An Overview of Near-Field Antenna Measurements," *IEEE Transactions on Antennas and Propagation,* **AP-34**, 1, January 1986, pp. 30-45.

4. D. Slater, "Near-Field Test Facility Design," Antenna Measurement Techniques Association Conference, 1985.

5. K. R. Grimm, "Antenna Analysis by Near-Field Measurements," *Microwave Journal*, **20**, 4, 1976, pp. 43-52.

6. W. Leach and D. Paris, "Probe Compensated Near-Field Measurements on a Cylinder," *IEEE Transactions on Antennas and Propagation*, **AP-21**, 4, July 1973, pp. 435-445.

7. A. C. Newell, "Error Analysis Techniques for Planar Near-Field Measurements," *IEEE Transactions on Antennas and Propagation,* **AP-36**, 6, June 1988, pp. 754-768.

8. A. D. Yaghjian, "Upper-Bound Errors in Far-Field Antenna Parameters Determined From Planar Near-Field Measurements. Part 1: Analysis," National Bureau of Standards Technical Note 667, Boulder, October 1975.

9. A. C. Newell and C. F. Stubenrauch, "Effect of Random Errors in Planar Near-Field Measurement," *IEEE Transactions on Antennas and Propagation*, **AP-36**, 6, June 1988, pp. 769-773.

10. J. C. Bolomey, O. M. Bucci, L. Casavola, G. D'Elia, M. D. Migliore, and A. Ziyyat, "Reduction of Truncation Error in Near-Field Measurements of Antennas of Base-Station Mobile Communication Systems," *IEEE Transactions on Antennas and Propagation*, **AP-52**, 2, February 2004, pp. 593-601.

11. O. M. Bucci and M. D. Migliore, "A New Method for Avoiding the Truncation Error in Near-Field Antennas Measurements," *IEEE Transactions on Antennas and Propagation*, **AP-54**, 10, October 2006, pp. 2940-2952.

12. A. C. Newell and D. Lee, "Application of the NIST 18 Term Error Model to Cylindrical Near-Field Antenna Measurements," Antenna Measurement Techniques Association Conference, Philadelphia, October 2000.

13. T. Isernia, G. Leone, and R. Pierri, "Radiation Pattern Evaluation from Near-Field Intensities on Planes," *IEEE Transactions on Antennas and Propagation*, **AP-44**, 5, May 1996, pp. 701-710.

14. R. G. Yaccarino, and Y. Rahmat-Samii, "Phaseless Bi-Polar Planar Near-Field Measurements and Diagnostics of Array Antennas," *IEEE Transactions on Antennas and Propagation*, **AP-47**, 3, March 1999, pp. 574-583.

15. S. F. Razavi and Y. Rahmat-Samii, "A New Look at Phaseless Planar Near-Field Measurements: Limitations, Simulations, Measurements, and a Hybrid Solution," *IEEE Antennas and Propagation Magazine*, **AP-49**, 2, April 2007, pp. 170-178.

16. R. Tkadlec and Z. Novacek, "Radiation Pattern Reconstruction from the Near-Field Amplitude Measurement on Two Planes Using PSO," *Radioengineering*, **14**, December 2005, pp. 63-67.

17. L. D. Bakhrakh and A. P. Kurochkin, *Holography in Microwave Engineering*, Moscow, S. Radio, (1979) (in Russian).

18. J. C. Bennett et al. "Microwave Holographic Metrology of Large Reflector Antennas," *IEEE Transactions on Antennas and Propagation*, **AP-24**, 3, May 1976, pp. 295-303.

19. I. V. Kaplun and A. P. Kurochkin, "Analysis of Random Errors in Holographic Technique Determination of Directional Antenna Characteristics," *Radiotekhnika i Elektronika*, **XX**, 10, October 1975, pp. 2038-2045.

20. D. Smith, M. Leach, M. Elsdon, and S. J. Foti, "Indirect Holographic Techniques for Determining Antenna Radiation Characteristics and Imaging Aperture Fields," *IEEE Antennas and Propagation Magazine*, **AP-49**, 1, February 2007, pp. 54-67.

21. V. Schejbal, *Microwave Antenna Near-Field Measurements*. PhD thesis, SAV Bratislava (Slovakia), 1979, (in Czech).

22. V. Schejbal, "Near-Field Antenna Measurement Using Holographic Method," *Slaboproudý obzor*, **39**, 9, September 1978, pp. 403-407 (in Czech).

23. V. Schejbal, "Accuracy of Near-Field Antenna Measurement Using Holographic Method," *Slaboproudý obzor*, **41**, 4, April 1980, pp. 182-186 (in Czech).

24. V. Schejbal and J. Honig, "Holographic Method of Near-Field Antenna Measurements," *10th European Microwave Conference*, Warszawa (Poland), 1980, pp. 167-171.

25. V. Schejbal and V. Kovarik, "Holography Methods for Antenna Near-Field Measurement," *Tesla Electronics*, **13**, 2, 1980, pp. 35-39.

26. V. Schejbal, "Numerical Simulation of Near-Field Antenna Measurement," *Tesla Electronics*, **13**, 3, 1980, pp. 67-72.

27. V. Schejbal and V. Kovarik, "Accuracy of Near-Field Antenna Measurement Using Holography," *Tesla Electronics*, **14**, 2, 1981, pp. 48-52.

28. V. Schejbal, "Numerical Simulations of Problems Occurring in Near-Field Antenna Measurements," 7th Colloquium on Microwave Communication, Budapest (Hungary), 1982, pp. 507-510.

29. V. Schejbal et al. "Czech Radar Technology," *IEEE Transactions on Aerospace and Electronics Systems*, **30**, 1, January 1994, pp. 2-17.

30. P. Bezousek and V. Schejbal, "Radar Technology in the Czech Republic," *IEEE Aerospace and Electronic Systems Magazine*, **19**, 8, August 2004, pp. 27-34.

Introducing the Feature Article Authors

Vladimir Schejbal graduated from the Czech Technical University, Prague, in 1970. He received the PhD degree from the Slovak Academy of Science, Bratislava, in 1980. He was with the Radio Research Institute Opocinek, the Czech Republic (Antenna Department) from 1969 to 1993. From 1983 to 1986, he was on leave with the Higher Institute of Electronics (Microwave Department) Beni Walid, Libya, as a lecturer. He has been with the University of Pardubice, the Czech Republic, since 1994, now as a full professor and a head of the department. He is interested in microwave antennas and propagation. He has published over 100 papers. He is a Senior Member of the IEEE.

Vlastimil Kovarik completed his studies at the Pardubice High School of Electrical Engineering, the Czech Republic, in 1970. He was with the Radio Research Institute Opocinek, the Czech Republic (Antenna Department) from 1970 to 1998. He has been with Retia a.s., Pardubice, since 1998. He is interested in radar antennas and propagation. He has published over 10 papers.

Dusan Cermak was born in 1974. He received his MS degree from the Czech Technical University in Prague in 2003, and his PhD degree from the University of Pardubice, the Czech Republic, in 2007. He has been with the University of Pardubice since 2003 as an Assistant Professor. He is interested in simulations, measurements, radar antennas, and propagation of electromagnetic waves. He has published over 20 papers.

Getting the *Magazine* by Air Freight

Air freight delivery of the *IEEE Antennas and Propagation Magazine* is available to subscribers in IEEE Regions 8-10. The cost is $44.00 per year. This can be added to a member's subscription (and the current cost verified) via the Web at http://services1.ieee.org/membersvc/addservices/intro.htm.

To All IEEE Life Members

Life Member status in the IEEE is an earned honor. Each year, most Life Members are sent a Life Member Profile in lieu of a membership dues invoice. **Life Members must return the Profile**, indicating that they wish to keep their membership(s) active, even if there are no changes. **If the profile is not returned, it is assumed that their membership should not be kept active, and they do not receive any complimentary Society publications to which they may be entitled.** If applicable, the complimentary Society publications that a Life Member would like to continue receiving must be indicated on the Profile. Life Members can still retain their membership in a Society, even if they do not wish to receive its publications. However, they *must* return the Profile.

The Profile can also be updated online at www.ieee.org/renewal, using an IEEE Web account. Those not having an IEEE Web account can register for one at www.ieee.org/web/accounts/.